ACS APPLIED MATERIALS & INTERFACES
Research Article
www.acsami.org

Dynamic Electrical Characteristics of Low-Power Ring Oscillators Constructed with Inorganic Nanoparticles on Flexible Plastics

Junggwon Yun, Kyoungah Cho,[†] and Sangsig Kim[†]

Department of Electrical Engineering, Korea University, Seoul 136-701, Korea

Supporting Information

ABSTRACT: In this study, we demonstrate for the first time the low-power and stable performance of a ring oscillator constructed on a flexible plastic with solution-processable inorganic nanoparticles (NPs). Our flexible ring oscillator is composed of three inverters based on n- and p-type inorganic NP thin-film transistors. Each of the component inverters exhibits a gain of ∼80 at a voltage of 5 V. For the ring oscillator, the sine waves are generated with a frequency of up to 12 kHz. The waveforms are undistorted under strained conditions and maintained even after 5000 bending cycles. The frequency and waveform of the output waves obtained from our flexible ring oscillator are analyzed and discussed in detail.

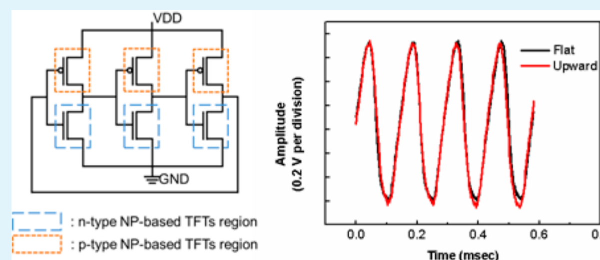

KEYWORDS: *II−VI semiconductor, electronic circuit, nanoparticle, flexible, ring oscillator, chalcogenide*

1. INTRODUCTION

Flexible printed electronics have become an emerging field in macroelectronics because of their unlimited potential allowing them to be applicable across a multitude of electronic products.[1−4] Up to now, organic semiconductors have been employed as the channel materials of flexible printed electronics by virtue of their solution processablility.[3−5] However, the inherent vulnerability of organic materials to moisture and heat hampers the development of flexible printed electronics, so different solution-processable materials are beginning to be used as an alternative to organic materials in the fabrication of flexible printed electronics.[6−11] Among the various solution-processable materials, inorganic nanoparticles (NPs) are particularly suited for the achievement of flexible printed electronics, owing to their chemical and physical stability. Previous studies on flexible thin-film transistors (TFTs) or logic devices constructed with solution-processable inorganic NPs have clearly demonstrated the static electrical characteristics of these flexible devices.[9−11] In order to expand the reach of flexible electronics, it is important to understand the dynamic electrical characteristics of devices made of solution-processable inorganic NPs. Therefore, in this study, we investigate for the first time the dynamic electrical characteristics and reliability of a flexible ring oscillator constructed with NP-based TFTs.

2. EXPERIMENTAL SECTION

2.1. Preparation of the Chalcogenide NPs. HgTe and HgSe NPs were used for the p-channel and the n-channel TFTs, respectively, in this study. HgTe becomes p-type because of Hg vacancies or Te interstitials and HgSe becomes n-type due to Hg interstitials and Se vacancies.[12,13] The NPs were synthesized by the colloidal method:[14] 1.98 g of $Hg(ClO_4)_2 6H_2O$ and 1 mL of 1-thoiglycerol in 250 mL of deionized water were prepared as the Hg^{2+} precursor solution. After being stirred and adjusted to pH 11.4 by adding 1 M NaOH, the Hg^{2+} precursor solution and the chalcogen precursor were placed in a separate three-neck flask connected by a septum.Three-tenths of a gram of Al_2Te_3 for HgTe NPs and 0.2 g of Al_2Se_3 for HgSe NPs were used for the chalcogen precursors, respectively. Before H_2Te (or H_2Se) gas was generated by the reaction of the chalcogen precursors and 4 M HCl under an N_2 atmosphere, the Hg^{2+} precursor solution was de-aerated by bubbling with N_2 for 30 min. H_2Te (or H_2Se) gas was then passed through the solution together with nitrogen flow for 30 min. The 1-thioglycerolcapped HgTe (or HgSe) NP solution was concentrated in a water bath at 60 °C using a rotary evaporator until its volume was reduced to 60 mL. After the addition of isopropyl alcohol, 1-thioglycerol-capped HgTe (or HgSe) NP powders were obtained by a centrifuge process. To remove the 1-thioglycerol used as a capping material, the powders were washed with acetone and methanol. Finally, the HgTe (or HgSe) NPs were dispersed in deionized water with a concentration of 0.1 mg/μl, and the solutions were used for spin-coating within a few hours in order to prevent aggregation resulting from the removal of 1-thioglycerol.

The synthesized HgTe and HgSe NPs were spherical in shape with their diameters of 4−7 nm, and they were highly crystalline with the zincblende lattice structures (see Figures S1 and S2 in the Supporting Information). Moreover, their bandgaps were extracted from the absorption spectra using Tauc formula,

$$\alpha h\nu = A(h\nu - E_g)^{1/2}$$

where α is the absorption coefficient, h is Planck's constant, ν is frequency, A is a constant, and E_g is the optical band gap energy. The photon energy ($h\nu$) vs $(\alpha h\nu)^2$ curves are plotted in Figure S3 of our Supporting Information. The bandgaps of HgTe and HgSe NPs were estimated from the curves to be 0.74 and 1 eV, respectively. For HgTe and HgSe semiconductors, the effective band gap is mostly determined by the shift of the conduction band toward higher energy with the

Received: July 27, 2012
Accepted: October 12, 2012
Published: October 12, 2012

 © 2012 American Chemical Society

shrinkage of their sizes to the nanoscales, since the effective mass of electron is much smaller than that of hole. Accordingly, the corresponding electron affinities of the HgTe and HgSe NPs are about 5.23 and 5.1 eV, respectively, as shown in Figure S4 in the Supporting Information.

2.2. Device Fabrication. A three-stage inverter-based ring oscillator was constructed with p- and n-type chalcogenide NPs (HgTe and HgSe NPs). Each of the component inverters was made with inverted-staggered TFTs on a polyethersulfone (PES) plastic substrate as follows: firstly, a cross-linked poly-4-vinylphenol film was spin-coated on a plastic substrate to enhance the adhesion between the substrate and the gold electrodes. Then, a gate electrode of gold (80 nm) was deposited by photolithography and thermal evaporation. The bottom-gate high-k dielectric Al_2O_3 film (∼15 nm) was formed by atomic layer deposition at 150 °C. The separated film regions of each NP were formed on the Al_2O_3 film by photolithography and spin-coating process. Before the spin-coating process of the aqueous NP-solutions on the patterned regions, O_2 plasma treatment was performed for 10 sec with an amplitude of 20 W to make the surface hydrophilic. Subsequently, an HgTe NP-film was formed by spin-coating at 7000 rpm for 40 s and annealed at 125 °C for 20 min to prevent the surface from having ambipolar characteristics. In contrast to the formation of the HgTe NP-film, the HgSe NP-film was formed without any annealing process to clearly show its gate-voltage-dependent properties. The surface morphologies of the HgTe and HgSe NP-films were taken with optical profiler (Figure S5 in the Supporting Information). Au metal source and drain electrodes (80 nm) were deposited with a channel length of 10 μm and width of 400 μm by photolithography and thermal evaporation. Three separated complementary inverters were completely fabricated. The connection between the inverters was completed by the deposition of Al lines. Figure 1 shows an optical image (a) and circuit diagram (b) of a representative ring oscillator. The electrical characteristics of the NP-based inverters were examined using an HP 4155C semiconductor analyzer at room temperature in air. AC input signals were created by a function generator (Agilent 81150A), and the frequency characteristics of the ring oscillator were demonstrated using an oscilloscope (Agilent MSO7052B). The bending tests were performed with a custom-built bending machine.

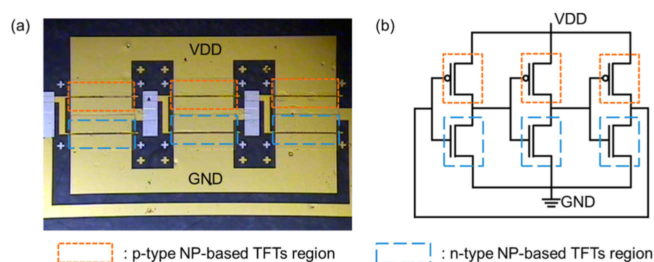

Figure 1. Optical image and corresponding circuit diagram of the NP-based flexible ring oscillator.

3. RESULTS AND DISCUSSION

Our 3-stage inverter-based ring oscillator is composed of three n-type and three p-type NP-based TFTs (Figure 1). These TFTs were characterized first before investigation of the ring oscillator. Representative HgSe and HgTe NP-based TFTs can be driven with a driving voltage lower than 2 V, and these TFTs exhibit typical n- and p-channel transfer characteristics (Figure 2); note that the leakage current is plotted in Figure 2 as a function of gate voltage. The driving voltage of the TFTs under study is remarkably reduced in magnitude compared with our previous report, in which the TFTs operate at driving voltages higher than 10 V.[10] The reduction of the driving voltage results from the decrease in the thickness of the gate dielectric layers by about a factor of three. The mobility and I_{on}/I_{off} ratio estimated from the transfer curves (Figure 2) are 1 cm^2/(V s) and 1 × 10^2 for the n-channel NP-based TFT, and 0.01 cm^2/(V s) and 1 × 10^2 for the p-channel NP-based TFT, respectively. The specific parameters of each NP-based TFT are indicated in Table 1. The mobility of the p-channel NP-based TFT is much lower than that of the n-channel NP-based one, causing distortion of the rectangular waves at the output stage, as will be demonstrated later.

Table 1. Parameters of the NP-Based TFTs

	I_{on}/I_{off}	μ (cm^2/(V s))	W/L	V_{TH} (V)	SS (V/dec)
p-channel NP-based TFT	1 × 10^2	0.01	40	0.2	1.37
n-channel NP-based TFT	1 × 10^2	1	40	0.8	0.78

The static and dynamic electrical characteristics of one of the three component NP-based inverters comprising our ring oscillator are examined here. The NP-based inverter exhibits excellent static transfer characteristics, with a maximum voltage gain of 80 at a V_{DD} of 5 V (Figure 3a). Although this gain is lower than those of the inverters using CNT (with a gain value of 58 at 1.5 V),[15] metal-oxide materials (with a gain value of 120 at 20 V),[16] and organic materials (with a gain value of 370 at 3 V),[17] the gain is higher than that of the ZnO NP-based inverter (with a gain value of 5.5 at 10−15 V).[18] Our inverter is superior to other NP-based inverters. Based on the static characteristics of the NP-based inverter, the dynamic characteristics are analyzed by examining the change of the output

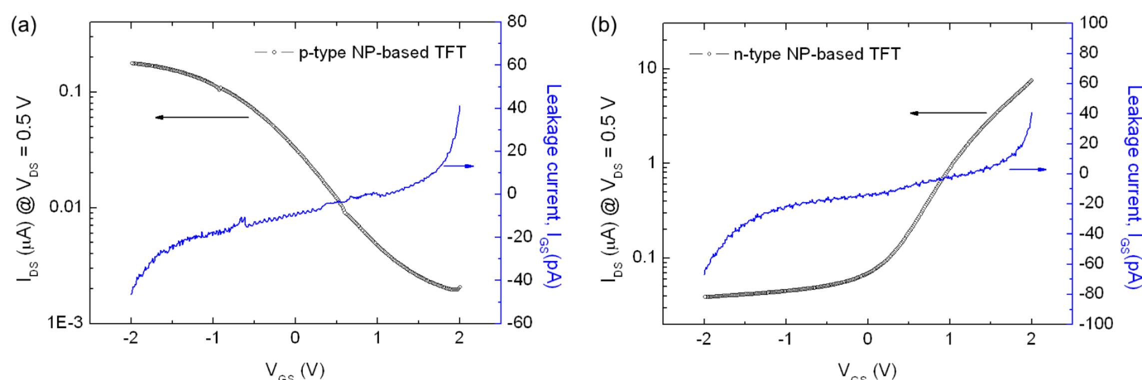

Figure 2. Electrical characteristics of the (a) p-channel and (b) n-channel NP-based TFTs.

dx.doi.org/10.1021/am301483u | ACS Appl. Mater. Interfaces 2012, 4, 5839−5843

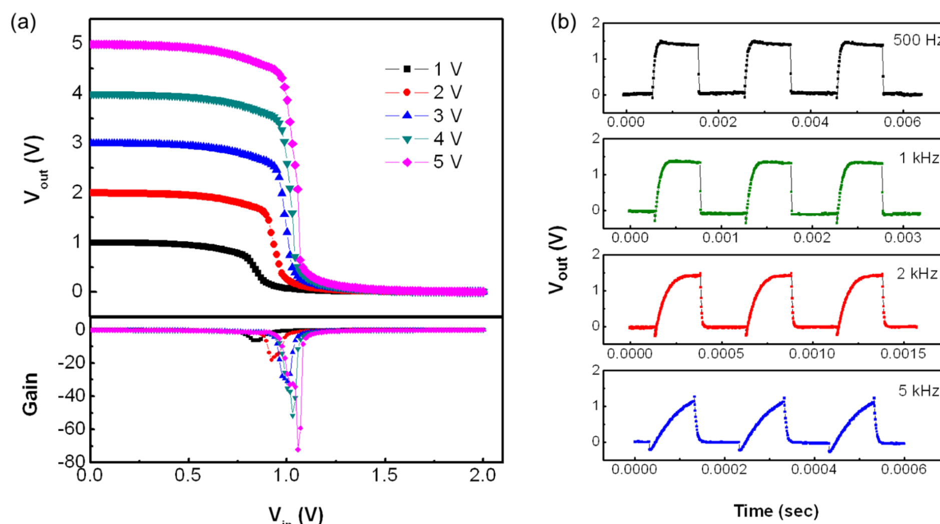

Figure 3. (a) Static and (b) dynamic characteristics of the NP-based complementary inverter. The dynamic characteristics show the change of the output waveform as a function of the input frequency with an amplitude of 2 V.

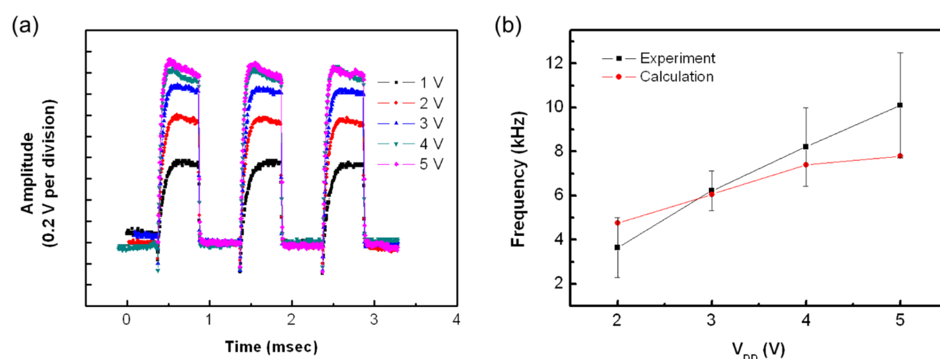

Figure 4. (a) Dependency of waveform distortion on the V_{DD} at 1 kHz. (b) Calculated and measured frequencies of the NP-based ring oscillator.

waveform as a function of the input frequency with an amplitude of 2 V (Figure 3b). As the input frequency is increased, the output waveforms become more distorted. The distortion of the rectangular wave at the output stage is attributed to the delay time of the inverter associated with the discharging/charging time of the load capacitance at the output. The discharging and charging times of the capacitance are determined by the mobilities of the n- and p-channel NP-based TFTs in the NP-based inverter, respectively. The slow propagation delay for the low-to-high transition is due to the relatively lower mobility of the p-channel NP-based TFT. Note that the mobility of the p-channel NP-based TFT is 10^2 times lower than that of the n-channel NP-based one. Thus, the difference between the mobilities of the p- and n-channel NP-based TFTs is responsible for the difference in the propagation delays between the low-to-high and high-to-low transitions.

The output waveforms of the NP-based inverter at the input in the case of continuous 1 kHz rectangular waveforms are depicted in Figure 4a. As the V_{DD} is increased, the propagation delay of the inverter is decreased from 70 to 40 μs. The frequency of the three-stage inverter-based ring oscillator can be estimated using the following equation[19]

$$f_{osc} = \frac{1}{n(\mathrm{tPHL} + \mathrm{tPLH})} \quad (1)$$

where n is the number of inverters, and tPHL and tPLH (extracted from Figure 4a) are the propagation delays for the high-to-low and low-to-high transitions, respectively. The calculated and measured frequencies are plotted in Figure 4b as a function of V_{DD}. The frequencies for 18 distinct ring oscillators were measured, and the maximum, the minimum, and the average values are exhibited. The large error bar between the maximum and the minimum is attributed to the variation of parasitic capacitance occurring in the ring oscillators. The parasitic capacitance results from the misalignment between the gate and source/drain electrodes. Our analysis reveals that the measured frequency is consistent with the calculated one, and that the frequencies are directly proportional to the applied bias. Our ring oscillator operates experimentally at frequencies ranging from 2 kHz to 12 kHz, which are comparable to those of other low-power flexible ring oscillators constructed with organic materials (~40 kHz at 3 V),[20] CNT (~2 kHz at 4 V),[21] or ZnO (~70 kHz at 5 V).[22]

On the other hand, the NP-based ring oscillators can have a tunable oscillation frequency, considering the relation between the frequency of the ring oscillator and the current, as shown in the following equation:

$$f_{osc} = \frac{I_{ctrl}}{2NC_G V_{osc}} \quad (2)$$

where I_{ctrl} is the current, N is the number of stages, V_{osc} is the amplitude, and C_G is the parasitic capacitance.[23] From the above equation, the frequency of the ring oscillator is proportional to the current, which flows in each of the

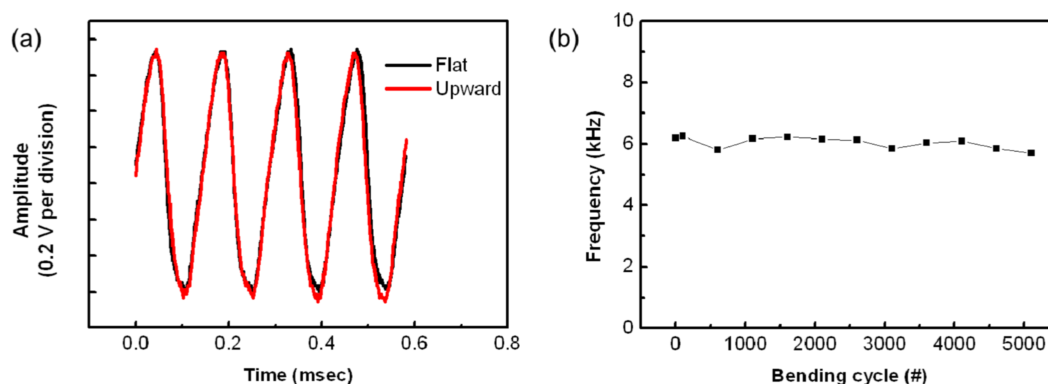

Figure 5. (a) Waveforms of the ring oscillator at 3 V under flat and 0.7% strain conditions. (b) Frequency variation as a function of the number of bending cycle.

component inverters. For NP-based ring oscillators, the magnitude of the current depends on the electrical properties of the NP-films, so that the frequency of the ring oscillator can be adjusted by changing their electrical properties. Among the various ways of changing the electrical properties of NP-films, the annealing process is a good solution. Notably, the HgSe NP-film used as an n-type channel material in this study shows an increase in the magnitude of the current with increasing annealing temperature.[10] To confirm the change of frequency in the NP-based ring oscillator, we post-annealed our ring oscillator at 115 °C. The post-annealed ring oscillator shows a frequency twice as high as that before post-annealing (see Figure S6 in the Supporting Information).

In this study, the flexibility of our ring oscillator is examined not only under bending condition with an upward strain 0.7% (see Figure S7 in the Supporting Information), but also as a function of the number of bending cycles, in which one cycle consists of the transition of the device from the flat to the upwardly bent state (and its return to the flat state). The magnitude of the strain is estimated from the following equation[9]

$$\text{strain} = \frac{(t_{\text{sub}} + t_{\text{film}})}{2R_c} \times 100 \tag{3}$$

where R_c, the bending curvature radius of the substrate, was 14 mm, and t_{sub} (the thickness of the PES substrate) and t_{film} (the total thickness of the film) were 200 μm and 400 nm, respectively.

The waveform of the three-stage inverter-based ring oscillator at a V_{DD} of 2 V is presented in Figure 5a. The normal sign wave is generated by a ring oscillator with a frequency of about 6 kHz, and the waveform is maintained without any distortion under an upward bending strain of 0.7%. The variation in the frequency of our representative ring oscillator at a V_{DD} of 2 V is plotted in Figure 5b as a function of the number of bending cycles. The initial frequency of the ring oscillator is maintained within a variation of 10% over 5000 bending cycles. These stable electrical characteristics are related to the stable operation of the flexible NP-based TFTs, as reported in a previous study.[11]

4. SUMMARY

In summary, we investigated for the first time the electrical characteristics of a 3-stage inverter-based ring oscillator composed of n- and p-type inorganic NP TFTs on flexible plastics. The component inverter exhibits a gain of ~80 at a voltage of 5 V. Our ring oscillator operates experimentally at frequencies ranging from 2 to 12 kHz, which is comparable with other ring oscillators constructed with organic, CNTs, or ZnO. The waveforms are undistorted under upward strain conditions of 0.7% and maintained even after 5000 bending cycles. The solution-processable inorganic NPs show suitability for future flexible printed electronics.

■ ASSOCIATED CONTENT

Supporting Information

TEM images of HgTe NPs and HgSe NPs (Figure S1), XRD patterns of the HgTe and HgSe NP-based films (Figure S2), bandgaps of the HgTe and HgSe NP-based films (Figure S3), energy diagrams of HgTe NPs and HgSe NPs (Figure S4), optical profiler images of the HgTe and HgSe NP-based films (Figure S5), change in frequency of NP-based ring oscillator after annealing (Figure S6), and schematic and photography of the upward bent sample (Figure S7). This material is available free of charge via the Internet at http://pubs.acs.org/.

■ AUTHOR INFORMATION

Corresponding Author

†Tel: +82-2-3290-3909 (K.C.); +82-2-3290-3245 (S.K.). Fax: +82-2-3290-3909 (K.C.); +82-2-3290-3894 (S.K.). E-mail: chochem@korea.ac.kr (K.C.); sangsig@korea.ac.kr (S.K.).

Notes

The authors declare no competing financial interest.

■ ACKNOWLEDGMENTS

This work was supported by the Future-based Technology Development Program (Nano Fields) and through the National Research Foundation of Korea (NRF) funded by the Ministry of Education, Science and Technology (2010-0019197) and the World Class University (WCU, R32-2008-000-10082-0).

■ REFERENCES

(1) Chen, P.; Fu, Y.; Aminirad, R.; Wang, C.; Zhang, J.; Wang, K.; Galatsis, K.; Zhou, C. *Nano Lett.* **2011**, *11*, 5301.
(2) Hübler, A.C.; Schmidt, G.C.; Kempa, H.; Reuter, K.; Hambsch, M.; Bellmann, M. *Org. Electron.* **2011**, *12*, 419.
(3) Xia, Y.; Zhang, W.; Ha, M.; Cho, J. H.; Renn, M. J.; Kim, C. H.; Frisbie, C. D. *Adv. Funct. Mater.* **2010**, *20*, 587.
(4) Baeg, K. J.; Khim, D.; Kim, D. Y.; Jung, S. W.; Koo, J. B.; You, I. K.; Yan, H.; Facchetti, A.; Noh, Y. Y. *J. Polym. Sci., Part B: Polym. Phys.* **2011**, *49*, 62.

(5) Herlogsson, L.; Colle, M.; Tierney, S.; Crispin, X.; Berggren, M. *Adv. Mater.* **2010**, *22*, 72.
(6) Dasgupta, S.; Kruk, R.; Mechau, N.; Hahn, H. *ACS Nano* **2011**, *5*, 9628.
(7) Noh, J.; Jung, M.; Jung, K.; Lim, S.; Lee, G.; Subramanian, V.; Leonard, A. D.; Tour, J.; Cho, G. *J. Appl. Phys.* **2010**, *108*, 102811.
(8) Nam, S. W.; Jiang, X.; Xiong, Q.; Ham, D.; Lieber, C. M. *Proc. Natl. Acad. Sci. U.S.A.* **2009**, *106*, 21035.
(9) Jun, J. H.; Park, B.; Cho, K.; Kim, S. *Nanotechnology* **2009**, *20*, 505201.
(10) Jang, J.; Cho, K.; Yun, J.; Kim, S. *Microelectron. Eng.* **2009**, *86*, 2030.
(11) Yun, J.; Cho, K.; Kim, S. *Nanotechnology* **2010**, *21*, 235204.
(12) Strauss, A. J.; Brebrick, R. F. *J. Phys. Chem. Solids* **1970**, *31*, 2293.
(13) Blue, M. D.; Kruse, P. W. *J. Phys. Chem. Solids* **1962**, *23*, 577.
(14) Rogach, A.; Kershaw, S.; Burt, M.; Harrison, M.; Kornowski, A.; Eychmuller, A.; Weller, H. *Adv. Mater.* **1999**, *11*, 552.
(15) Ha, M.; Xia, Y.; Green, A. A; Zhang, W.; Renn, M. J.; Kim, C. H; Hersam, M. C.; Frisbie, C. D. *ACS Nano* **2010**, *4*, 4388.
(16) Dindar, A.; Kim, J. B.; Fuentes-Hernandez, C; Kippelen, B. *Appl. Phys. Lett.* **2011**, *99*, 172104.
(17) Martens, S. C.; Zschieschang, U.; Wadepohl, H.; Klauk, H.; Gade, L. H. *Chem.—Eur. J.* **2012**, *18*, 3498.
(18) Wolff, K.; Hilleringmann, U. *Solid-State Electron.* **2011**, *62*, 110.
(19) Na, J. H.; Kitamura, M.; Arakawa, Y. *Appl. Phys. Lett.* **2008**, *93*, 213505.
(20) Zschieschang, U.; Kang, M. J.; Takimiya, K.; Sekitani, T.; Someya, T.; Canzler, T. W.; Werner, A.; Jan, B. N.; Klauk, H. *J. Mater. Chem.* **2012**, *22*, 4273.
(21) Sun, D. M.; Timmermans, M. Y.; Tian, Y.; Nasibulin, A. G.; Kauppinen, E. I.; Kishimoto, S.; Mizutani, T.; Ohno, Y. *Nat. Nanotechnol.* **2011**, *6*, 156.
(22) Zhao, D.; Mourey, D. A. *IEEE Electron Device Lett.* **2010**, *31*, 323.
(23) Retdian, N.; Takagi, S.; Fujii, N. *Proc. IEEE Asia-Pacific Conf.* **2002**, 201.